Synthesis and characterization of Al doped ZnO powder by precipitation method

S. I. Inamdar[a*], G. J. Navathe [a], S. V. Malgaonkar [a], C. J. Kamble [a], M. M. Karanjkar [a*].

[a*]Department of Physics, Vivekanand College, Kolhapur

Abstract: Structural, optical and dielectrical properties of ZnO and aluminum doped ZnO (Al:ZnO) powder synthesized by simple and convenient chemical precipitation method have been reported.. The powders were characterized by variety of experimental techniques such as X-ray diffraction (XRD), thermal analysis TG-DTA, dielectrical measurements and so on. It was observed that annealing removes the impurities and enhances the purity of ZnO nanoparticles. To understand the conduction mechanism, complex impedance measurements were carried out as a function of applied frequency. The complex impedance spectra show that as Al doping increases the total impedance (Z´ and Z´´) decreases. Room temperature dielectric properties viz. relative dielectric permittivity (ε´) and dielectric loss (tan δ) for the samples were studied as a function of frequency (20 Hz to 1 MHz). These studies indicate that dielectric permittivity goes on increasing with increase of Al doping.

Keywords : Al:ZnO, XRD, complex impedance and dielectric properties etc.

Introduction : Nanomaterials have great importance because of their small particle size and large surface area. Due to such remarkable properties these materials are used in optoelectronic and electronic nanodevice.[1] Among the various semiconductor nanomaterials ZnO is the best promising candidate because of its wide band gap 3.37eV and high exciton binding energy 60meV at room temperature [2]. ZnO is the II-IV group semiconductor and usually it adopts hexagonal wurtzite crystal structure. It has crystal structure similar to the gallium nitride (GaN), whose band gap is 3.3eV at 300k[3] another wide gap semiconductor material. Due to such wide gap this type of materials are used in optoelectronic applications[4] .But ZnO has some advantages over GaN such as high band gap and high exciton binding energy as mentioned above.

There are many advantages of zinc oxide such as, abundance in earth crust, non toxicity, low material cost, chemically stability, and high transparency in the visible and near infrared region.[5] ZnO get customary attention because of its special properties such as its chemical activity, and novel optical , mechanical , electromagnetic, thermodynamic, and electrodynamic properties which gives wide range of applications.[6] such as photocatalysis [7], gas sensor[8], visible blind or solar blind photodetector[9] etc. The physical and chemical properties of ZnO nanoscale particle are different when compare with the bulk materials. ZnO nanopowder when

controlled to nanosize show atom like behavior which results from higher surface energy. It is due to large surface area and wider band gap between the conduction and valance band[10]

There are many method which had reported for the synthesis of ZnO nanopowder such as decomposition [11], sol gel method[12] , precipitation method[13], hydrothermal method[14], combustion method[15],molten salt method[16] and so on. This study is carried out by using the precipitation method for the preparation of ZnO powder by using zinc chloride as precursor solution, and addition of aqueous ammonia to adjust the pH of the solution. The crystalline size and morphology of ZnO powder depends on the synthesis method. They have the main influence on the properties of ZnO powder [17]. In this report chemically precipitated ZnO powder is discussed for various thermal and morphological characterizations.

2. Experimental: Pure and aluminium doped ZnO powder can be prepared by precipitation method. In this study AR grade equimolar zinc chloride hexahydrate, aluminium nitrate and ammonium hydroxide solution is used. The preparation conditions were carefully controlled. Double distilled water was used for solution preparation. Solution pH, considered using the relation between pH and concentrations of both the solutions was adjusted to neutral by adding aqueous ammonia to preserve the hydroxide phases of Zn. 0.1M zinc chloride was dissolved in double distilled water and stirring the solution vigorously by adding drop wise aqueous ammonia to adjust the pH of the solution equal to 7.Then white gelatinous precipitate formed, was filtered using Whatmann filter paper No.17. The precipitate was washed thoroughly. It was further dried at ambient temperature and sintered at different temperatures within 400-1000°C for 5 hr in air atmosphere. These compositions were further mixed with polyvinyl alcohol as a binder and pressed into pellets of 10mm diameter and 2–4mm thickness using a hydraulic press. The flow chart for synthesis of material is given in Fig.1.
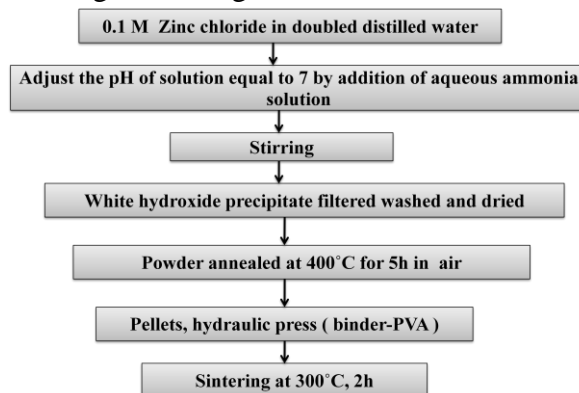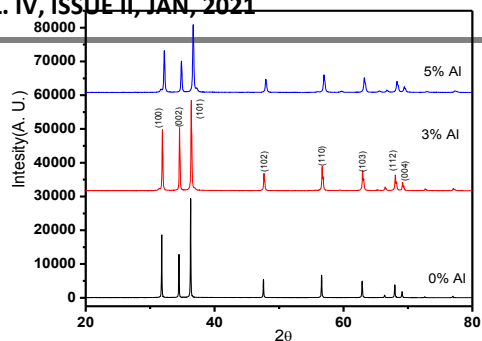

Fig. 1 Material synthesis of flow chart

The powders were characterized by X-ray diffractometer (Brukar D2 phaser) using Cu K$_\alpha$ radiation (λ = 1.54056 Å) for structural analysis. The frequency dependence of dielectric permittivity (ε'), dissipation factor (tanδ) and complex impedance in the range from 20Hz to 1MHz were studied using a precision LCR meter bridge (HP 4284 A).
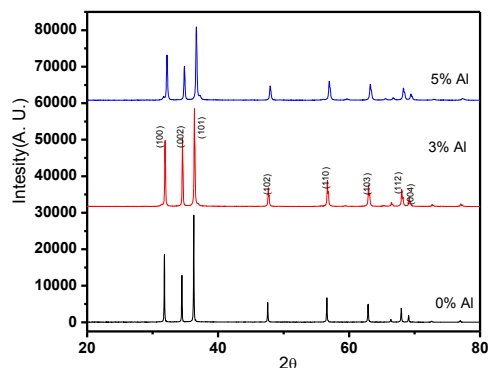
3. Result and discussion:
3.1 XRD analysis:

Fig. 2 . X-ray diffraction patterns of ZnO powder synthesized by precipitation technique at various Al doping   concentration.

Fig.2 shows the shows the X-ray diffraction patterns of ZnO powder synthesized by precipitation technique at various Al doping concentration. The samples are polycrystalline in nature and shows hexagonal crystal structure (JCPDS card no. - 01-079-0206). The XRD pattern shows lattice planes (1 0 0), (0 0 2), (1 0 1), (1 0 2), (1 1 0), (1 0 3), (1 3 2), (0 0 4). The highest intensity of lattice plane (1 0 1) . The crystallite size (D) was calculated from XRD pattern by using Scherrer's formula [18],

$$D = \frac{0.9\lambda}{\beta cos\theta} \qquad (1)$$

Where β the broadening of diffraction line measured at half of its maximum intensity (rad) FWHM and λ is the X-ray wavelength (1.5406 A°).

The preferential orientation of the films is studied by calculating the texture coefficient TC $_{(hkl)}$ for all the planes using the equation,

$$TC = \frac{I_{hkl}/I_o}{(1/N)\sum(I_{hkl}/I_o)} \qquad (2)$$

Where $TC_{(hkl)}$ is the texture coefficient of the *(hkl)* plane, *I* the measured intensity, *Io* is the standard intensity. And *N* is the number of planes observed in the X-ray diffraction pattern. The deviation of the texture coefficient from unity implies the preferred orientation of the growth of the films. The TC for (1 0 0), (0 0 2) and (1 0 1) planes shown in table 1.

The standard deviation (σ) is calculated to explain the growth mechanism, by using the equation $\sigma =$

$$\frac{\sum I_{hkl}^2 - (\sum I_{hkl})^2 / N}{N} \qquad (3)$$

Where, I stand for relative intensity of the *(hkl)* plane. It is seen that (Table 1) the substrate temperature has made a small change in σ values, which reflects the onset of homogenous nucleation.

X-ray diffractograms shows no appreciable effect of solution concentration on the crystal structure of ZnO, but it is observed in pattern that there is shift in after Al doping in ZnO powder. The intensities of (1 0 1) diffraction peak relative to (1 0 0) and (0 0 2) declines as doping concentration increase from 0% to 5%. ZnO grows along the (1 0 1) direction. The values of crystallite size, texture coefficient and slandered deviation shown in Table 1.

(h k l)	2Θ(°)	d spacing (A°)	Crystallite size (in nm)	Texture coefficient (TC)
(1 0 0)	31.6778	2.8229	24.58832	0.4425
(0 0 2)	34.1601	2.62267	24.74603	4.604231
(10 1)	36.1594	2.48212	13.39857	0.331657

Table:1 XRD parameters for Al doped ZnO powder

The crystallite size of ZnO powder increase with increase in Al doping concentration. The texture coefficient and standard deviation of ZnO powder decrease for 3% Al doping and decrease for further increase in doping concentration.

3.2 TG-DTA analysis: To know the decomposition and phase formation that occurs during the heating treatment of the as prepared compound, the thermal analysis is carried out in the temperature range of 30°C to 1000°C. The TGA-DTA curve for the typical precursor is as shown in Fig.3
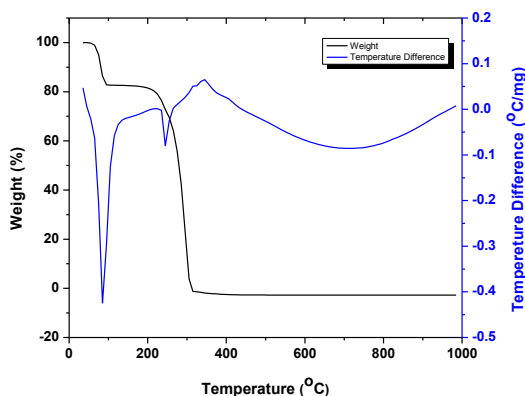

Fig. 3 TG-DTA curve of the precursor: According to TG curve the precursor loses its weight in two major steps. The first major step is in the temperature below the 100°C and indicated a loss

of 16.93% revealing the hydrogenation process of surface adsorbed water molecules [19]. The second step of weight loss 84.08% appeared in the temperature range 100˚C-250˚C.Above the temperature 310˚C the TG curve remains constant. The total weight loss in the entire thermal study is indicating the major amount of ZnO formation during the synthesis.

The DTA curve of the precursor obtained during thermal treatment exhibits two endothermic peaks which corresponds to two major weight loss steps of the TGA curve, and one exothermic peak. The first endothermic peak between 50˚C-100˚C can be associated with the removal of surface water of the sample with weight loss of 16.93%. The weight loss 84.08% corresponding to one endothermic and one exothermic peaks in the temperature range 220˚C-350˚C.

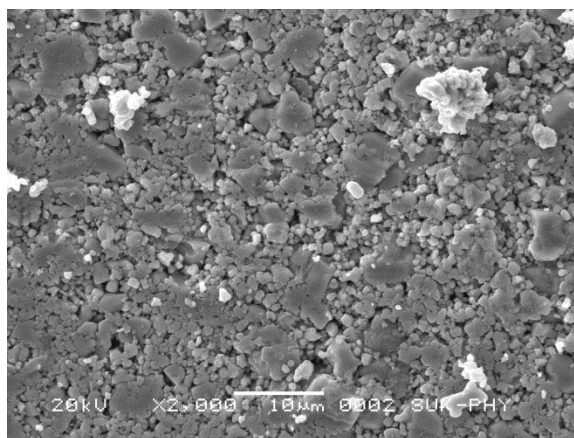### 3.3 Surface morphological study:

Fig. 4 scanning electron micrograph of pure ZnO powder

Figure 4 shows the SEM micrograph of ZnO powder pillet. This ZnO powder can be prepared by precipitation method and then transferred into the pillets by using hydraulic press. As shown in figure SEM showed a close packed morphology uniform for ZnO powder. The grain like dense structure is observed in the SEM of ZnO powder. This type of morphology is used for many applications of ZnO powder like gas sensor [20] and so on.

3.4 Elemental and chemical composition analysis: Figure 5 shows the EDAX spectrum of 0%, 3% and 5% Al doped ZnO powder. EDAX spectrum reveals the presence of Zn, O and Al element in the sample. From the spectrum it can be seen that the amount of Al element in the sample goes on increasing as doping concentration increased in the ZnO powder
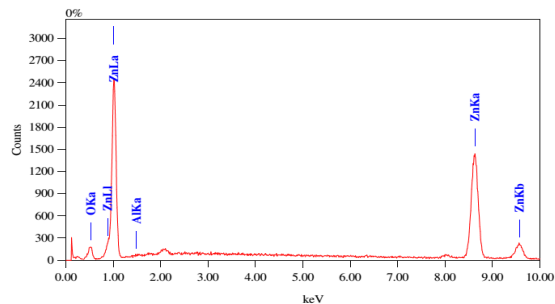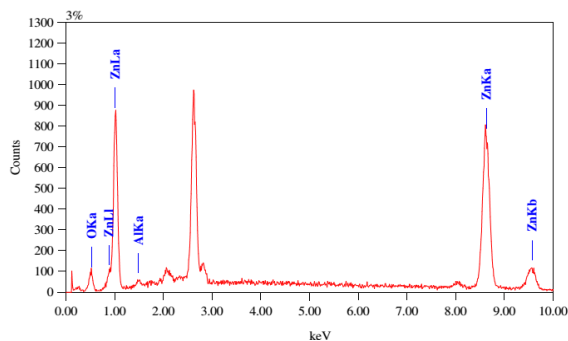
Fig. 5(a) EDX for pure ZnO thin films

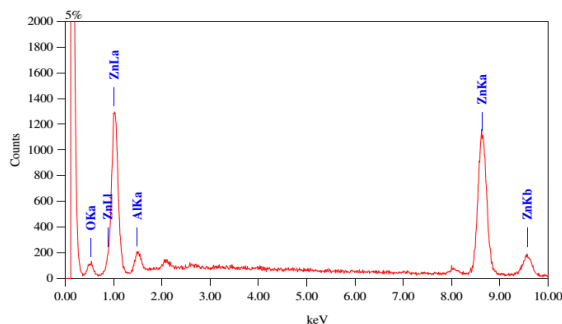**Fig. 5 (b) EDX for 3%**

Al doped ZnO thin films.

Fig. 5(c) EDX for 5% Al doped ZnO thin films

The elemental analysis for each element Zn, O and Al for each sample (O%, 3% and 5% doping) is as shown in table 2. Except Zn, O and Al, no other peak from any element found in the spectrum which confirmed that the formation of pure Al doped ZnO powder.

Element	Mass %		
	0%	3%	5%
O	1.93	1.67	1.01
Al	0.02	0.66	1.44
Zn	98.06	97.67	97.55

Table: 2 Mass % of O, Al, and Zn as determined by EDX analysis

3.5 Dielectrical Properties: The frequency dependence of the Dielectric permittivity (ε') for all the samples was studied at room temperature.
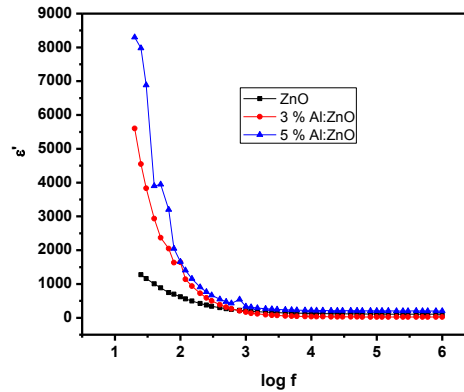

Fig. 6 Variation of room temperature dielectric constant with frequency

The fig.6 shows the variation of dielectric permittivity with frequency. The dielectric permittivity decreases with increase in frequency from 20Hz to 1MHz showing usual dielectric dispersion behavior at low frequencies the dispersion of dielectric permittivity is large while it is independent of frequency beyond 100 kHz. As frequency increase, ionic and orientation sources of polarizability decreases and finally disappear due to the inertia of molecules and ions. In practice there is a relaxation time for charge transport and therefore the dielectric permittivity depends on the applied frequency. The observed variation in dielectric permittivity can be explained on the basis of space charge polarization [21] and is governed by no. of space charge carried and resistivity of the samples. The charge carries, which take part in ion exchange, can be produced during the sintering process. Similar results were observed for other samples. The permittivity is directly proportion to the square root of conductivity. The permittivity is high at low frequencies and decrease as frequency increases. The decrease in permittivity takes place when the jumping frequency of electric charge carriers con not follow the attention of the applied AC electric field beyond a certain critical frequency.
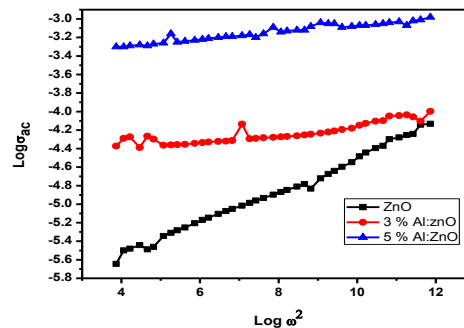
3.6 AC Conductivity:

Fig. 7 Variation of dc electrical resistivity with temperature

The variation of AC conductivity as function of frequency is represented in fig 7. It is observed that ac conductivity at room temperature reveals increasing trend of AC conductivity with frequency. The reason for this increasing trend should be searched in the frequency dependence of small polaron hopping conduction. It should be recalled that the conduction at lower temperature is due to impurities and defects while at higher temperature it is intrinsic property of the material. For ionic and low energy band solids, the conduction is better explained in terms of small polaron [22]. The excess electrons in a narrow conduction band (or excess holes in a narrow valence band) due to their interaction with lattice ions distort the surrounding in such a way that the potential well thereby generated is deep enough to introduce localization leading to the formation of polaron. Polarons are divided into two categories: (i) large polarons and (ii) small polaron. If the conduction is due to large polarons, it can be explained on the basis of band mechanism at all temperatures.
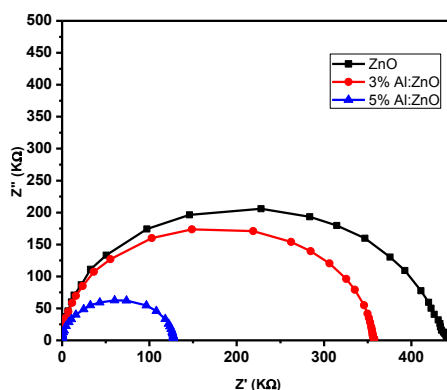
3.7 Impedance spectroscopy:
Fig. 8 Impedance spectra of Al doped ZnO powder

Complex impedance spectroscopy method is widely used to measure the electrical properties of the materials and their interface with electrically conducting electrodes. This spectroscopic technique separates the resistive (real) and reactive (imaginary) components of the electrical parameters. The complex impedance spectroscopy is measured by the relation. [23]

$$Z^* = Z' - iZ'' = R_s - \frac{1}{j\omega C_s} \quad (5)$$

The electrical phenomenon (due to bulk material, grain boundary) and interfacial phenomenon appears in the form of arc of a semicircle, when real verses imaginary part of impedance are plotted called Nyquist plots as shown in fig. 8. The impedance spectrum is analyzed by the change in the diameter of the semicircle but not its shape. Intersect of the semicircle with the real axis at lower frequency side is attributed to the total resistance (the sum of the resistance of grains and grain boundaries) while at higher frequency it is due to the grain impedance response (resistance of grains only) [23]. The grain boundary resistance decreases with increase in Al doping concentration in ZnO. Also the value of Z' decreases with increase in Al doping concentration indicating that grain size increases with increases in doping concentration and ultimately grain boundary resistance

becomes decreases. This has helped to lowering the barrier to the motion of charge carriers causing increased electrical transport.

Conclusions: In this study, the effect of Al doping concentration on structural, dielectric and impedance properties of ZnO powder have been studied. The XRD peaks shifts towards higher 2θ values prove that incorporated impurity Al atoms enters in ZnO lattice at Zn sites. Both dielectric constant and dielectric loss increases with increases of Al doping concentration. The complex impedance spectra suggest a grain boundary contribution in the conduction process. The total impedance (Z', the real axis intercept at low frequency side) and imaginary part of complex impedance (Z") of all samples is decreased with increase in concentration.

References:

1. B. C. Yadav, R. Srivastava, A. Kumar, Characterization of ZnO Nanomaterial Synthesized by different methods, International Journal of Nanotechnology and Applications 2 (2007) 1-11

2. M. Chitra, K. Uthayarani, N. Rajasekaran, E. K. Girija, Preparation and characterisation of Al doped ZnO nanopowders, Physics Procedia 49 (2013) 177 –182

3. U. Ozgur, Ya.I. Alovov, C.Liu, A. Teke,M.A.Reshchikov, S. Dogan, V. Avrutin, S.J. Cho, H. Morkoc, A comprehensive review of ZnO materials and devices, Journal Of Applied Physics 98 (2005) 041301

4. R.J. Chung, H.Y. Wang, Y.C. Li, P.H. Yeh, Preparation and Sensor Application of Carbon Coated Zinc Oxide Nanorods Array, Journal of The Australian Ceramic Society 49 [2] (2013) 81 – 88

5. L. Znaidi, T. Touam, D. Vrel, N. Souded , S.B. Yahia, O. Brinza, A. Fischer, A. Boudrioua, AZO Thin Films by Sol-Gel Process for Integrated Optics, Coatings 3 (2013) 126-139

6. M. Thirumavalavan, K.L. Huang, J.F. Lee, Preparation and Morphology Studies of Nano Zinc Oxide Obtained Using Native and Modified Chitosans, Materials 6 (2013) 4198-4212

7. M. Nirmala, M. G. Nair, K. Rekha, A. Anukaliani, S.K. Samdarshi, R.G. Nair, Photocatalytic Activity of ZnO Nanopowders Synthesized by DC Thermal Plasma, African Journal of Basic & Applied Sciences 2 (2010) 161-166

8. S.M. Kanan, O. M. El-Kadri, I.A. Abu-Yousef ,M. C. Kanan, Semiconducting Metal Oxide Based Sensors for Selective Gas Pollutant Detection, Sensors 9 (2009) 8158-8196

9. S.I. Inamdar, K.Y. Rajpure, High-performance metal–semiconductor–metal UV photodetector based on spray deposited ZnO thin films, Journal Of Alloys And Compound 595 (2014) 55-59

10. Y. T. Prabhu, K. V. Rao,V. S. Sai Kumar, B. S. Kumari, Synthesis of ZnO Nanoparticles by a Novel Surfactant Assisted Amine Combustion Method, Advances in Nanoparticles 2(2013) 45-50

11. Y. Dimitriev, M. Gancheva, R. Iordanova, Synthesis Of ZnO By Mechanochemical Decomposition Of Zinc Carbonate Hydroxide, Journal of the University of Chemical Technology and Metallurgy 46 (2011) 243-248

12. T. Ates, C. Tatar, F. Yakuphanoglu, Preparation of semiconductor ZnO powders by sol– gel method: Humidity sensors, Sensors and Actuators A 190 (2013) 153-160